Significant FRET between SWNT/DNA and Rare Earth Ions: A Signature of Their Spatial Correlations

Tetyana Ignatova,[†] Hikmat Najafov,[†,∥] Aleksandr Ryasnyanskiy,[†] Ivan Biaggio,[†] Ming Zheng,[§] and Slava V. Rotkin[†,⊥,*]

[†]Department of Physics, Lehigh University, 16 Memorial Drive East, Bethlehem, Pennsylvania 18015, United States, [§]National Institute of Standards and Technology, 100 Bureau Drive, Gaithersburg, Maryland 20899, United States, [⊥]Center for Advanced Materials and Nanotechnology, Lehigh University, 5 E. Packer Avenue, Bethlehem, Pennsylvania 18015, United States, and [∥]Current address: Advanced Crystal Group, Coherent Inc., 31 Farinella Drive, East Hanover, New Jersey 07936, United States

ABSTRACT Significant acceleration of the photoluminescence (PL) decay rate was observed in water solutions of two rare earth ions (REIs), Tb and Eu. We propose that the time-resolved PL spectroscopy data are explained by a fluorescence resonance energy transfer (FRET) between the REIs. FRET was directly confirmed by detecting the induced PL of the energy acceptor, Eu ion, under the PL excitation of the donor ion, Tb, with FRET efficiency reaching 7% in the most saturated solution, where the distance between the unlike REIs is the shortest. Using this as a calibration experiment, a comparable FRET was measured in the mixed solution of REIs with single-wall nanotubes (SWNTs) wrapped with DNA. From the FRET efficiency of 10% and 7% for Tb and Eu, respectively, the characteristic distance between the REI and SWNT/DNA was obtained as 15.9 ± 1.3 Å, suggesting that the complexes are formed because of Coulomb attraction between the REI and the ionized phosphate groups of the DNA.

KEYWORDS: single-wall nanotubes · photoluminescence spectroscopy · fluorescence resonance energy transfer · time-resolved spectroscopy · rare earth ions

In the past decade significant interest was demostrated in the resonance energy transfer in condensed matter, biological and hybrid organic−inorganic systems.[1−6] The energy transfer allows efficient energy harvesting in natural photosynthesis systems as well as in man-designed materials. Complex nanoscale samples, *e.g.*, interacting biomolecules[7] or single-atom dopants used for enhancement of semiconductor materials properties,[8] can be studied with a subwavelength resolution by optical techniques utilizing the energy transfer. This requires a resonant coupling of an object of interest with a known, well-characterized system. Lanthanide ions can be such a reference system not only because of their unique luminescent properties, *i.e.*, long lifetimes, narrow bands, and large oscillator strengths, but also because of the simple chemistry of their organic compounds. Indeed, the energy transfer *via* the resonance exchange mechanism was demonstrated between lanthanide ions in solution[9−12] and in the solid state.[13−16] Subsequently biofunctionalized Tb^{3+} and Eu^{3+} rare earth ions were successfully applied as optical probes to study DNA structure.[17,18]

Optical properties of both functionalized and pure SWNT materials, including their photoluminescence (PL), were studied extensively.[19−30] Recently the resonance energy transfer (RET) has been measured in SWNT materials: between different SWNT species in the nanotube bundles,[31−39] from atomic oxygen adsorbed on a SWNT,[40] and from polymers,[41,42] encapsulated oligomers,[43] fluorescent dye,[44] and an organic (porphyrin) molecule complex.[45,46]

Not only do the nanoscale complexes of SWNTs with various substances show interesting optical properties, but these complexes may enable sensors, solar cells, and other applications.[47−49] Yet little is known about the actual physical structure of nanocomplexes and how they form. Thus we aimed our work on developing a technique for studying correlations between SWNTs and species interacting in solution. In the case of strong interactions, such as covalent bonding, their effect can be readily traced, by a strongly quenched PL signal, for example. The SWNTs in our experiments are well shielded by the DNA wrap, which eliminates the possibility of direct chemical functionalization. More subtle interactions and nonbonded spatial correlations, such as formation of ionic shells around SWNTs in solution, are hard to detect in general. Ions may not produce a significant effect on the nanotube itself until completely associated, *e.g.*, after drying on its surface. Methods granting

* Address correspondence to rotkin@lehigh.edu.

Received for review May 24, 2011 and accepted June 24, 2011.

Published online June 24, 2011
10.1021/nn201911b

© 2011 American Chemical Society

access to such information dynamically and *in situ* would be especially valuable to study the kinetics of nanocomplex formation. The results presented below demonstrate that the FRET technique allows quantifying the degree of long-range correlation between the multivalent REIs and SWNT/DNA macroions. Furthermore, the measured average distance between the interacting species proves that the origin of the correlation is the electrostatic interaction at the nanoscale.

The paper is organized as follows. We will discuss two different sets of FRET measurements: (1) between unlike REIs, Tb^{3+} and Eu^{3+}, and (2) between SWNTs and each of these REIs. We will show that these species have similar spectral overlaps, which allows one to gain knowledge on the FRET distances by comparing them side by side. First we will demonstrate that the Tb lifetime shortening in the mixed solution with Eu has its origin in the energy transfer from the Tb donor ion to Eu acceptor. Then the similar time-dependent data for the SWNT–REI solution are analyzed. Additional evidence for Tb–Eu FRET is provided next by presenting the PL of the acceptor directly induced by the resonantly excited donor. After establishing a reliable calibration for the FRET distance in the Tb–Eu solution, the spatial correlation between SWNT and REIs is studied as a function of the concentration of the species. The conclusions and details on the materials and experimental methods will follow.

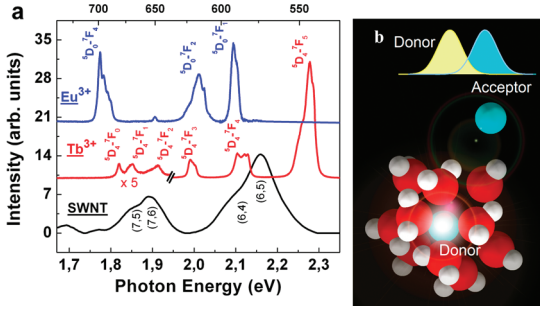

Figure 1. (a) Superimposed PL spectra of REI in solution: pure Tb^{3+} emission (red curve) at 488 nm wavelength excitation, pure Eu^{3+} emission (blue curve) at 514 nm wavelength excitation, and SWNT optical absorption spectrum (black curve). The baselines were offset for clarity. (b) Sketch of the first coordination sphere of a solvated REI, surrounded with the partially oriented water molecules and spatially isolated from another ion. Inset shows that for efficient FRET between the ions, a strong spectral line overlap is required, in addition to the short distance.

RESULTS AND DISCUSSION

Time-Resolved PL Spectroscopy. Steady-state PL of pure REI solution as well as the visible-range absorption of the SWNT/DNA solution is presented in Figure 1a (see Materials and Experimental Methods section for preparation details and Supporting Information for SWNT NIR absorption data). Each of the PL bands of the REI is labeled with the corresponding transition in the single ion, while the broadening is likely due to the interaction with the water solvation shells of the ion (schematically shown in Figure 1b). For the large FRET a spectral overlap between the PL and absorption lines is needed, as seen in Figure 1 and further quantified in Figure 2d–f.

Time-resolved spectroscopy following excitation by 20 ps long laser pulses of selectively (resonantly) excited Tb^{3+} ions in the $TbCl_3$ water solution (green curve in Figure 2a) showed a typical PL lifetime of the pure REI: $\tau_{Tb}{}^0 \approx 0.395$ ms, for example, for the strongest $^5D_4$–$^7F_5$ transition at 2.28 eV (544 nm), the highest PL band in the middle red curve in Figure 1a. Other lines show a similar lifetime. In the mixed solution that

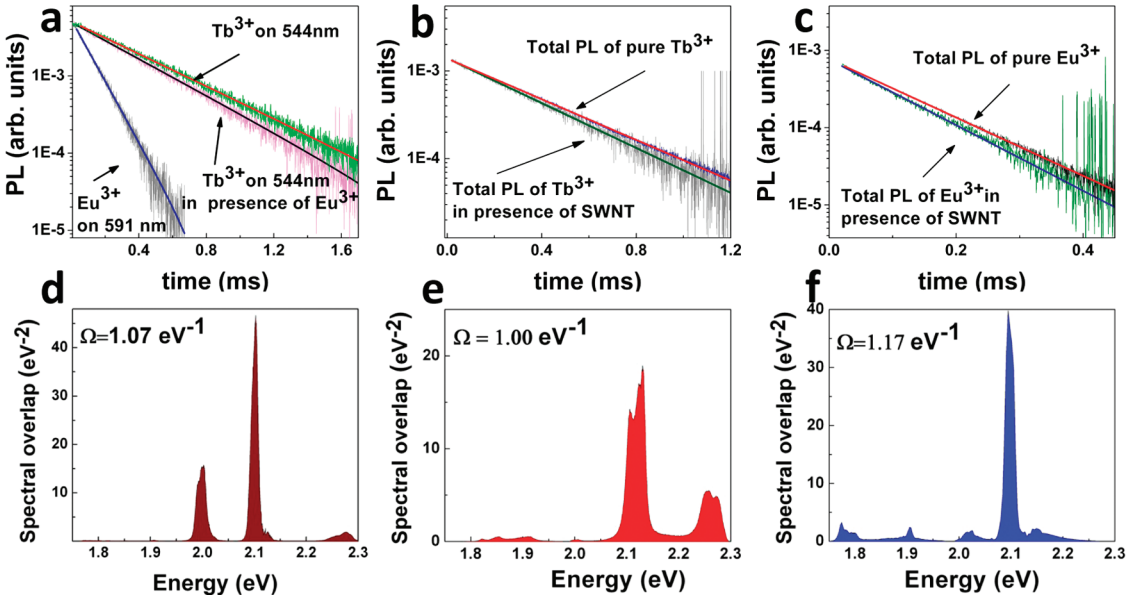

Figure 2. Time-resolved PL for (a) pure REIs and their mixed solution, (b) pure Tb and Tb–SWNT mixed solution, and (c) pure Eu and Eu–SWNT mixed solution. Spectral overlaps for (d) Tb with Eu; (e) SWNTs with Tb; and (f) SWNTs with Eu.

contained both Tb^{3+} and Eu^{3+} ions we observed systematic shortening of the Tb decay time: $\tau_{Tb}^{Eu} \approx$ 0.366 ms (pink curve in Figure 2a). Shortening of the PL lifetime may be attributed to the increase of radiative and/or nonradiative rates. The increase of the radiative rate can be rejected because we did not observe an increase of the PL efficiency, which would result from a faster radiative recombination. The latter mechanism is possible, and it may be due to a strong interaction with the polar water molecules. However, this interaction with water is present even in the pure solution where the REIs are surrounded by solvation shells (Figure 1b). The coupling is unlikely to strengthen in the mixed solution, where the solvation shell may become only distorted. In fact it was observed earlier that the nonradiative decay rate becomes lower when the REI–water solvation structure is influenced by another substance or the REI is partially shielded from the water.[50] Then we have to assume an additional nonradiative channel appears, which can be FRET. Eu emission (gray curve in Figure 2a) also demonstrates the longer decay time, $\tau_{Eu}^{Tb} \approx 0.111$ ms (compared to the lifetime in the pure solution, $\tau_{Eu}^{0} \approx 0.109$ ms, not shown), compatible with the same FRET rate for the Tb acting as a "feeding" source.

The resonance mechanism of the energy transfer is based on the dipole interaction between an excited state of a donor and a ground state of the acceptor atom/molecule, which can be related to the dipole transition matrix element of interaction, H_{int}, and the optical densities of the donor and acceptor molecules. Within the Förster model,[51,52] the temporal variation of the emission of the sensitizer (donor) must shorten due to the activator (acceptor). The magnitude of the transfer efficiency is given by

$$W_{AB} = 1 - \tau_A^B/\tau_A^0$$

where τ_A^B and τ_A^0 are the decay time of the sensitizer A in the presence of the activator B and the radiative lifetime of the pure sensitizer, respectively. In the case of the Tb^{3+}/Eu^{3+} system shown in Figure 2a the corresponding transfer efficiency is about 7%.

Existence of FRET requires an appreciable overlap between the spectral lines of the emitting and receiving species. The overall transfer efficiency, W_{AB}, depends on the mutual spectral overlap, Ω, between the line shape functions of the optical transitions, $g_A(h\nu)$ and $g_B(h\nu)$. The Ω is given by the integral term of the following expression:

$$W_{AB} = \frac{(2\pi)^2}{h^2\tau_A^B} |\langle A^*B|H_{int}|AB^*\rangle|^2 \int g_A(h\nu)\, g_B(h\nu)\, dh\nu$$

where ν is the frequency, h is the Planck constant, and H_{int} is the interaction Hamiltonian. A unique characteristic of the trivalent rare earth ions is such that the electron–phonon coupling of all the transitions that take place within the 4f manifold is very weak; that is,

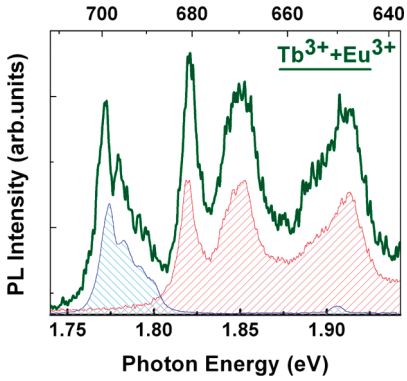

Figure 3. PL emission of the mixed solution containing both REIs (green curve) at 488 nm excitation (Tb resonant wavelength excitation). The transfer-mediated emission line from Eu^{3+} at 699 nm is superimposed with the PL emission of a solution of pure Tb (red) or pure Eu (blue), excited at 488 or 514 nm, respectively.

no Stokes shift between the emission and photoexcitation spectra is expected. Therefore, the line shape of the radiative transitions is approximately the same as for the reciprocate transition (absorption line). Then the overlap of the two spectra in Figure 1a allows one to evaluate the FRET between Tb and Eu. Numerical convolution of the area under the curves gives an appreciable overlap between the spectra of Tb and Eu ions in the energy region 1.75–2.35 eV (Figure 2d).

Using REIs as a reference for the calibration, next we measured the shortening of Tb and Eu emission in the presence of ssDNA/SWNT. Indeed, decay times of the observed REI lines demonstrate similar substantial shortening as an indication of the FRET from a REI to the SWNT. The emission data for the mixed solution were collected both through the monochromator and without it to measure the FRET at the wavelength corresponding to the peak of emission or the total PL intensity of the donor. The lifetime shortening was almost the same for all of the REI PL bands. Thus we present in Figure 2b the decay time of the total PL from the pure Tb and from the mixed solutions of Tb/SWNT (at the resonant wavelength excitation for Tb). The $TbCl_3$ and SWNT concentrations were 0.2 mM and 4 mg/L, respectively. Figure 2c shows the corresponding PL data for pure Eu and Eu/SWNT mixed solution (with the same concentrations: 0.2 mM and 4 mg/L), excited at 525 nm, the resonant wavelength excitation for Eu. The decay time shortening corresponds to the FRET transfer efficiency of 10% and 7% for Tb and Eu, respectively. The magnitudes of Ω in Figure 2e,f are also comparable with the spectral overlap between Tb and Eu in Figure 2d.

FRET-Mediated Acceptor Emission. If the shortening of decay time in Figure 2a is due to FRET between Tb and Eu, one should be able to verify it by measuring the induced PL. Indeed, in Figure 3 we provide the direct observation of the energy transfer by steady-state PL spectroscopy. The mixed solution was excited selectively at a wavelength of 488 nm, which fits only the

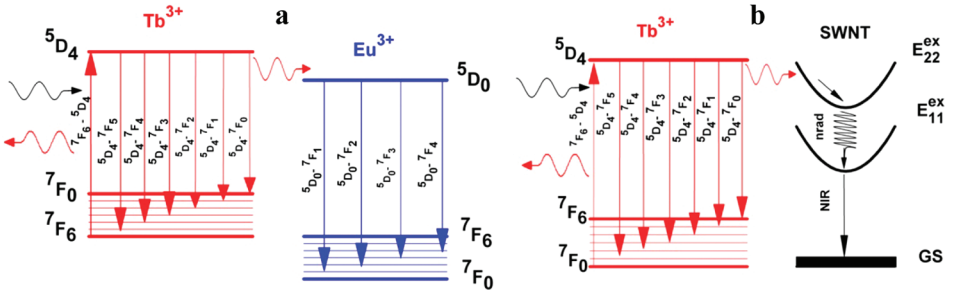

Figure 4. FRET energy level diagram: (a) between Tb and Eu ions, (b) between Tb and SWNT.

Tb^{3+} ion and does not fit any excitation line for the Eu^{3+} ion. The FRET-mediated emission line $^5D_0-^7F_4$ from the Eu^{3+} is evident in the spectra at $h\nu = 1.77$ eV ($\lambda = 699$ nm). For comparison, on the same graph we present the PL spectra of the pure Tb solution (red curve), showing no PL in the same range (the spectral lines of Tb^{3+} emission are seen above 1.8 eV), and the pure Eu solution (blue curve), demonstrating the same band $^5D_0-^7F_4$ for Eu^{3+} transition. The FRET energy level diagram for Eu and Tb ions is shown in Figure 4a. Given this qualitative confirmation of the FRET, we were further able to provide the quantitative estimate *via* the spectral weights of the PL bands of Tb and Eu. Fitting the PL intensity of the mixed solution (green curve in Figure 3) with the weighted PL spectra of the pure solutions (red and blue curves) we obtained partial contributions of the REIs. Taking into account that the concentrations of Tb and Eu were the same in the mixed solution but the quantum efficiency of Eu is slightly lower, as detailed below, and assuming a lossless internal conversion of the transferred energy into $^5D_0-^7F_4$ radiative transition, we estimated the FRET-induced PL efficiency to be ~10%, comparable with the one obtained from the lifetime shortening.

Even though the same energy transfer mechanism is responsible for PL lifetime shortening in the REI/SWNT solution, one cannot observe FRET-induced PL from the SWNTs in the visible range. This is due to the SWNT charge carriers, after excitation in the second subband, E_{22}^{ex}, experiencing a fast nonradiative intersubband relaxation into the lowest subband, E_{11}^{ex}, during 10−20 fs (Figure 4b), followed by a longer radiative and nonradiative relaxation to the ground state.[53] Thus the efficiency of SWNT PL in the visible range, E_{22}^{ex}, is negligible small. We were able to observe SWNT infrared emission from the E_{11}^{ex} levels in a separate experiment. Figure 5 shows PL spectra of the mixed solution with $TbCl_3$ (red) compared with the PL from the pure SWNT/DNA solution (blue, normalized to the main (6,5) peak intensity). Three extra PL peaks are evident, which we attribute to the transfer-mediated emission from (8,3), (7,5), and (7,6) SWNTs at 968, 1038, and 1138 nm, respectively, using our absorption data (see Supporting Information) as well as the PL/PLE map shown in the upper inset of Figure 5.

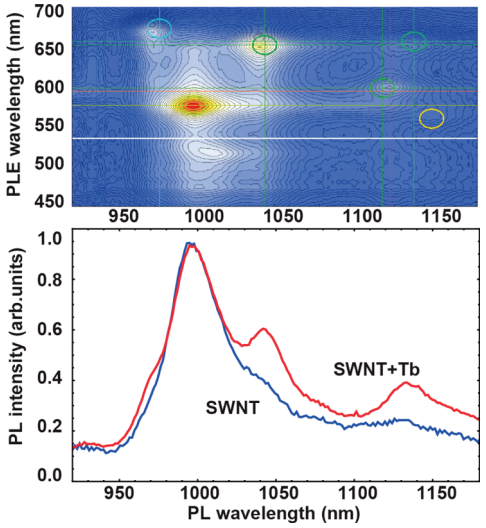

Figure 5. PL (blue) and FRET-induced PL (red) emission of the SWNT/DNA solution (mainframe). (Upper inset) PL/PLE map of the pure SWNT solution with thin lines and circles denoting separate chiralities, following the literature data. White line corresponds to the PL (blue curve in the mainframe) at the Tb resonant wavelength excitation at 532 nm (2.33 eV). The PL FRET-induced emission of several SWNTs that cannot be resonantly excited at 532 nm is clearly seen as 3 peaks on the PL from the mixed solution (red curve).

We conclude that the overlap with the Tb emission line at ~1.9 eV (~650 nm) can explain off-resonant excitation of these three SWNT species (compare the position of the horizontal white line of the excitation at 2.33 eV and original positions of the resonant peaks of these SWNTs in the upper inset of Figure 5).

Spatial Correlation Analysis. The time-resolved measurements were repeated for solutions with different relative concentrations of REIs and SWNTs. In Figure 6 we plot representative data for increasing SWNT content in the mixed solution, from the left to the right. Black squares/triangles correspond to the pure concentrated terbium/europium solution: [SWNT] = 0, [Tb or Eu] ≈ 1.2 M. Upon adding SWNTs to the pure solution, we observe a significant decrease of the lifetime but also large scatter of the data (red circles and blue triangles in Figure 6a for Tb and purple pentagons for Eu in Figure 6b). We attribute the scatter to the fact that the sample is not uniform anymore. Indeed REI and SWNT have opposite charges in solution. The

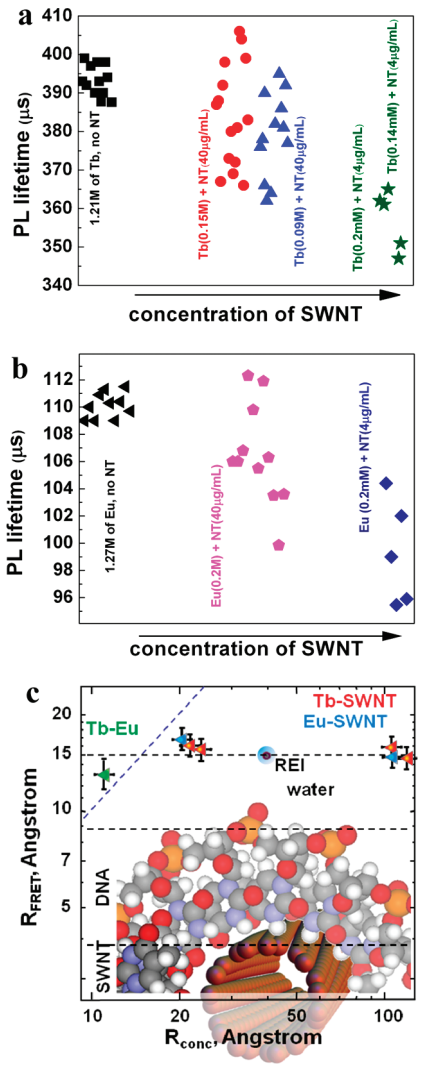

Figure 6. (a) PL lifetime of the pure Tb solution and the SWNT mixed solution as a function of relative concentration of SWNT (activator). (b) Same for Eu. (c) Cross-correlation plot of the sensitizer−activator distance as determined from the FRET *vs* the distance derived from the concentration of the species. Note the double logarithmic scale. Dashed diagonal line shows the cross-correlation for the noninteracting components; dashed horizontal lines represent SWNT, DNA, and water shell excluded volumes from bottom to top. Background image shows geometry of the complex with the water molecules removed for clarity.

ionization of the DNA backbone results in a significant negative total surface charge density of the SWNT/DNA hybrid. Positive REIs should be attracted by this negatively charged surface. Thus the pair-correlation function for the REI should be greatly enhanced near the surface, as compared to the noninteracting species. We stress that these solutions with the low SWNT content still contain REIs in excess to the SWNT/DNA surface charge, and only a fraction of REIs are bound. In contrast, a significant amount of Tb/Eu ions are free. Since we excited and probed the solution within the focus area of our setup and, after adding REI, the solution became nonuniform due to the SWNT coalescence, in different measurements we were able to probe the volumes that contain more REI bound to the SWNT/DNA surface or those where the free REI ions dominate the PL response. Thus one should observe a distribution of the lifetimes with two limiting values, given by fully solvated (free) REIs and by partially correlated (bound) REIs. These measurements already indicated the existence of two different lifetimes in the solution, due to free and bound REIs, even though additional experiments were designed with the higher relative concentration of SWNTs. For example, a solution with [Tb] = 0.14−0.2 mM and [SWNT] = 4 mg/L has shown single PL decay time (green stars in Figure 6a), which was attributed to the Tb−SWNT/DNA complex only. We speculate that these samples had a concentration of Tb corresponding (or close) to the saturation of the charge of the DNA/SWNT as expected from the DNA backbone charge density. The observed difference between free Tb PL lifetime (black symbols), 0.395 ± 0.005 ms, and the one in the complex (green stars), 0.350 ± 0.005 ms, gives the 10% FRET efficiency. Very similar results for Eu bound to SWNT/DNA in the mixed solution with [Eu] = 0.2 mM and [SWNT] = 4 mg/L has shown a FRET efficiency of 7% (dark blue diamonds in Figure 6b).

We emphasize that in the REI−SWNT system, upon lowering the concentration of the REI sensitizer by more than 3 orders of magnitude as compared to the set of experiments with two unlike REIs, not only does the FRET remain observable but also its efficiency persists at the same level, which cannot be expected for a simple noninteracting solution. The extraordinarily high FRET efficiency (for a relatively low concentration of the SWNT activator) requires additional attention. Another essential parameter of the energy transfer is the critical, or Förster, distance, R_c. The transfer efficiency can be expressed as

$$W_{AB} = 1/(1 + R^6/R_c^6)$$

where R is the distance between emitting and receiving species and R_c is the Förster distance when the FRET efficiency is 50%. This distance depends on the optical parameters of the system as

$$R_c = \left(\frac{3 f_{SWNT} h \Omega \eta_{REI} e^2}{4k^4 n^4 4\pi\varepsilon_0 mc}\right)^{1/6}$$

where Ω is the spectral overlap, ε_0 is the vacuum permittivity, e and m are the electron charge and mass, c is the speed of light, h is the Planck constant, η_{REI} is the quantum yield of PL of the sensitizer, f_{SWNT} is the oscillator strength of the receiving species (SWNT or Eu ion) at the wavevector $k = \omega/c$, and the angular resonance excitation frequency is $\omega = 2\pi\nu$. The Förster distance for Eu is known: $R_c \approx 10$ Å (an average value taken from the literature[54,55]). For SWNT we evaluate it *via* the oscillator strength:

$$f_{SWNT} = \frac{2\varepsilon_0 mc}{\pi e^2} \frac{9n}{(n^2+2)^2} \sigma(\omega)\Delta\omega$$

where the refractive index (part of the Onsager–Lorentz factor) is taken as $n = 1.4$ for the water solution, and $\sigma(\omega)\Delta\omega$ is the acceptor absorption cross section times the bandwidth of the transition. Using the average absorption cross section of SWNTs, $\sigma \approx (0.73-1.8) \times 10^{-17}$ cm^2/atom (literature values from refs 56–60), and $\Delta\omega \approx 30$ meV (fit to our data) we estimate the SWNT average oscillator strength to be $(1.6-3.95) \times 10^{-3}$, which is consistent with the previous studies.

The PL quantum yield of REI sensitizers was experimentally measured (see Supporting Information). Rhodamine 6G ethanol reference solution with a known 100% PL quantum yield was used to calibrate the spectra. We obtained $\eta_{Tb} = 1.3\%$ and $\eta_{Eu} = 0.8\%$, which are the typical values for REI water solutions.[61] We derive $R_c \approx 10.9 \pm 0.8$ Å for Tb/SWNT solution and $\sim 10.4 \pm 0.8$ Å for Eu/SWNT solution. We note that despite the uncertainty in f_{SWNT}, due to the averaging over the SWNT ensemble and relatively large range of σ, the Förster distance cannot substantially change because it has a weak (power of 1/6) dependence on the materials' optical parameters according to the equation above.

Following this simple calculation we obtain an estimate for $R \approx 14 \pm 2$ Å for FRET in the Tb–Eu system. On the other hand, in $TbCl_3$ and $EuCl_3$ solutions with the concentration $c = 1.2$ M, the minimum distance between unlike REIs in the mixed solution is approximately 11 Å. This number is in good agreement with the one obtained from the FRET efficiency between Tb and Eu. However the REIs showed a negative correlation due to the Coulomb repulsion between positively charged ions, that is, a smaller FRET efficiency than the one expected for an ideal noninteracting solution. Indeed the Tb–Eu data point (green triangle in Figure 6c), averaged over multiple measurements of the FRET efficiency, is above the dashed diagonal line corresponding to the noninteracting components.

The nominal distance between the species for Tb/SWNT and Eu/SWNT solutions obtained from their concentrations, R_{conc}, is an order of magnitude larger than for the Tb–Eu case, even though we measured a very strong FRET signal that corresponds to the average distance for the REI–SWNT case $R \approx 14.6-17.2$ Å, plotted on the vertical axis in Figure 6c. Thus the data points for Tb–SWNT (red) and Eu–SWNT (blue) solutions are well below the diagonal dashed line for the noninteracting components. We speculate that this is possible only in the case of formation of REI–SWNT complexes due to the electrostatic attraction between the negatively charged DNA backbone (ionized phosphate groups) and positively charged REIs in the water solution. A similar interaction is known to result in a fast ion condensation on the surface of the DNA rods, changing the ion pair correlation function, significantly reducing the spacing, and making the FRET possible.

The obtained value for R is in agreement with the proposed geometrical size of the complex, shown in the inset of Figure 6c. The radius of the SWNT/DNA hybrid is expected to be ~9–11 Å (DNA thickness ≈ 5.1 Å from ref 30), and the width of the REIs' solvation shell should be added. The first coordination sphere of the solvation water molecules is at ~2.5 Å for typical REIs, and it is at ~4.5 Å for the second coordination sphere. Thus the critical distance evaluated from the exclusion volume argument (dashed horizontal line in Figure 6c) is consistent with the measured one from the FRET and is much smaller than the distance between the noninteracting species from the known concentrations of initial solutions (dashed diagonal line).

CONCLUSIONS

In conclusion, FRET was measured in the mixed solutions of unlike REIs (Tb and Eu) as well as in solutions of each of these ions with the DNA wrapped SWNTs. The FRET was detected by shortening of the REI lifetime with time-resolved PL as well as with directly induced PL spectroscopy.

The characteristic distance between the donor and acceptor species has been derived from the measured FRET efficiency. Our study revealed a negative correlation (the repulsion with the longer distance) for the Tb–Eu case and significant positive correlation (the attraction and the complex formation) for the REI–SWNT/DNA case. The data are in good agreement with the theoretical estimates and allow proposing REIs and their FRET as a sensitive tool for detecting the kinetics of the interaction of SWNTs in aqueous solutions.

MATERIALS AND EXPERIMENTAL METHODS

For the sample preparation we used $EuCl_3$ and $TbCl_3$ REI salts dissolved in deionized (DI) water. Emission spectra of Tb^{3+}, resonantly excited at 488 nm (red curve), and Eu^{3+}, resonantly excited at 514 nm (blue curve), shown in Figure 1a were taken with a Horiba JY U1000 Raman spectrometer and with an Ar laser as the excitation source.

We assign each of the PL "bands" (broad lines with a fine structure) to a transition between D and F manifolds of the REI, additionally displaced by a local field, most likely due to the water environment around a particular solvated ion. Each REI is known to form a complex with 8 or 9 water molecules in solution (Figure 1b), and there is an even longer correlation beyond this first water solvation shell. The fine structure of the spectral lines is reproducible. Final assignment of the spectral lines and a sketch of the corresponding transitions between energy levels can be found in Figures 1a and 4a, respectively.

A solution of SWNTs wrapped with single-stranded DNA (ssDNA) was prepared from "as produced" CoMoCat material from Carbon Nanotechnologies Inc. (Houston, TX) and $(GT)_{20}$ DNA, custom-made by Integrated DNA technologies, Inc.

(Coralville, IA). Before the measurements, the solution of SWNT wrapped with the ssDNA was centrifuged using a Microcon spin filter YM100 (Millipore) and resuspended in DI water with an appropriate concentration to remove the trace of the original buffer. This procedure is similar to that described elsewhere.[62] SWNT absorption (Figure 1a) was taken by a Perkin-Elmer Lambda 2 spectrophotometer in the visible spectral range that covers optical transitions in the E_{22}^{ex} excitonic manifolds. Only E_{22}^{ex} excitons are in resonance with the REI emission spectra in the energy range of $E = 1.9-2.2$ eV. The absorption data show that the most abundant species are the tubes (6,5), (6,4), (7,6), and (7,5), further confirmed by near-infrared absorption data (see Supporting Information) and the PL/PLE map of Figure 5, inset, consistent with the earlier studies of CoMoCat SWNTs.[63,64] The SWNT PL/PLE map was taken by a JY-Horiba nanolog-3 spectrofluorometer with a liquid nitrogen cooled InGaAs detector.

Time-resolved PL experiments were performed by detecting the PL transients excited by wavelength tunable 20 ps laser pulses at a repetition rate of 10 Hz. The wavelength of the laser pulses was tuned to resonantly excite the REIs and the PL was detected by a photomultiplier connected to a digital oscilloscope.

Acknowledgment. This work was partially supported by a Lehigh University FIG grant. The authors thank Dr. J. Fagan, Dr. D. Pristinski, and Dr. C. Khripin (NIST) for valuable discussions and technical help.

Supporting Information Available: Additional details on the near-infrared absorption of the pure SWNT/DNA solution, calculation of the quantum yield of the REIs solutions, and supplementary figures, tables, and reference. This material is available free of charge *via* the Internet at http://pubs.acs.org.

REFERENCES AND NOTES

1. Engel, G. S.; Calhoun, T. R.; Read, E. L.; Ahn, T.-K.; Mancal, T.; Cheng, Y.-C.; Blankenship, R. E.; Fleming, G. R. Evidence For Wavelike Energy Transfer through Quantum Coherence in Photosynthetic Systems. *Nature* **2007**, *446*, 782–786.
2. Scholes, G. D. Quantum-Coherent Electronic Energy Transfer: Did Nature Think of It First? *J. Phys. Chem. Lett.* **2010**, *1*, 2–8.
3. Jang, S. Theory of Coherent Resonance Energy Transfer for Coherent Initial Condition. *J. Chem. Phys.* **2009**, *131*, 164101–164112.
4. Chang, H.; Tang, L.; Wang, Y.; Jiang, J.; Li, J. Graphene Fluorescence Resonance Energy Transfer Aptasensor for the Thrombin Detection. *Anal. Chem.* **2010**, *82*, 2341–2346.
5. Hennebicq, E.; Beljonne, D.; Curutchet, C.; Scholes, G. D.; Silbey, R. J. Shared-Mode Assisted Resonant Energy Transfer in the Weak Coupling Regime. *J. Chem. Phys.* **2009**, *130*, 214505–214505-6.
6. Ma, B.; Xu, M.; Zeng, F.; Huang, L.; Wu, S. Micelle Nanoparticles for FRET-Based Ratiometric Sensing of Mercury Ions in Water, Biological Fluids and Living Cells. *Nanotechnology* **2011**, *22*, 065501.
7. Santoso, Y.; Joyce, C. M.; Potapova, O.; Le Reste, L.; Hohlbein, J.; Torella, J. P.; Grindley, N. D. F.; Kapanidis, A. N. Conformational Transitions in DNA Polymerase I Revealed by Single-Molecule FRET. *Proc. Natl. Acad. Sci. U. S. A.* **2010**, *107*, 715–720.
8. Park, J. H.; Steckl, A. J. Demonstration of a Visible Laser on Silicon Using Eu-Doped GaN Thin Films. *J. Appl. Phys.* **2005**, *98*, 056108–3.
9. Tanner, P. A.; Wang, J. Energy Transfer From Gd^{3+} to Tb^{3+} in Solution. *Chem. Phys. Lett.* **2008**, *455*, 335–338.
10. Wang, J.; Tanner, P. A. Energy Transfer and Photoextinction from Ln^{3+} to Tb^{3+} and Eu^{3+} in Aqueous Chloride Solutions. *J. Lumin.* **2008**, *128*, 1846–1850.
11. Guo, Z.; Yson, R. L.; Patterson, H. H. Tunable Energy Transfer between Luminescent Nanoclusters and Rare Earth Ions in Aqueous Solution. *Chem. Phys. Lett.* **2007**, *433*, 373–378.
12. Guo, Z.; Yson, R. L.; Patterson, H. H. Solvent Dependent Tunable Energy Transfer of D10 Metal Dicyanide Nanoclusters with Eu^{3+} and Tb^{3+} Rare Earth Ions. *Chem. Phys. Lett.* **2007**, *445*, 340–344.
13. Holloway, J. W. W.; Kestigian, M. Energy Transfer between the Sm^{3+}, Eu^{3+}, Tb^{3+}, and Dy^{3+} Ions in Sodium Rare-Earth Tungstates. *J. Opt. Soc. Am.* **1966**, *56*, 1171–1171.
14. Blasse, G.; van den Heuvel, G. P. M.; Van Dijk, T. Energy Transfer from Gd^{3+} to Tb^{3+} and Eu^{3+}. *Chem. Phys. Lett.* **1979**, *62*, 600–602.
15. Verwey, J. W. M.; Dirksen, G. J.; Blasse, G. A Study of the Eu^{3+} Charge-Transfer State in Lanthanide-Borate Glasses. *J. Non-Cryst. Solids* **1988**, *107*, 49–54.
16. Najafov, H.; Kato, A.; Toyota, H.; Iwai, K.; Bayramov, A.; Iida, S. Effect of Ce Co-Doping on $CaGa_2S_4$: Eu Phosphor: I. Energy Transfer from Ce to Eu Ions. *Jpn. J. Appl. Phys.* **2002**, *41*, 1424–1430.
17. Klakamp, S. L.; Horrocks, W. D. Lanthanide Ion Luminescence as a Probe of DNA Structure. 1. Guanine-Containing Oligomers and Nucleotides. *J. Inorg. Biochem.* **1992**, *46*, 175−192 and 193−205.
18. Peng, Y.; Song, Y.; Feng, L.; Ren, J.; Qu, X. 7-Amino Actinomycin D Bound to Single-Stranded Hairpin DNA Enhanced by Loop Sequence-Dependent Luminescent Eu^{3+} and Tb^{3+} Binding. *J. Inorg. Biochem.* **2009**, *103*, 1675–1679.
19. Jorio, A.; Dresselhaus, M. S.; Dresselhaus, G. *Carbon Nanotubes: Advanced Topics in Synthesis, Properties, and Applications, Topics in Applied Physics*; Springer: Berlin, 2008; Vol. 111.
20. O'Connell, M. J.; Bachilo, S. M.; Huffman, C. B.; Moore, V. C.; Strano, M. S.; Haroz, E. H.; Rialon, K. L.; Boul, P. J.; Noon, W. H.; Ma, J.; *et al.* Band Gap Fluorescence from Individual Single-Walled Carbon Nanotubes. *Science* **2002**, *297*, 593–596.
21. Bachilo, S. M.; Strano, M. S.; Kittrell, C.; Hauge, R. H.; Smalley, R. E.; Weisman, R. B. Structure-Assigned Optical Spectra of Single-Walled Carbon Nanotubes. *Science* **2002**, *298*, 2361–2366.
22. Lebedkin, S.; Hennrich, F.; Skipa, T.; Kappes, M. Near-Infrared Photoluminescence of Single-Walled Carbon Nanotubes Prepared by the Laser Vaporization Method. *J. Phys. Chem. B* **2003**, *107*, 1949–1956.
23. Tan, P. H.; Hasan, T.; Bonaccorso, F.; Scardaci, V.; Rozhin, A. G.; Milne, W. I.; Ferrari, A. C. Optical Properties of Nanotube Bundles by Photoluminescence Excitation and Absorption Spectroscopy. *Phys. E (Amsterdam, Neth.)* **2008**, *40*, 2352–2359.
24. Lefebvre, J.; Homma, Y.; Finnie, P. Bright Band Gap Photoluminescence from Unprocessed Single-Walled Carbon Nanotubes. *Phys. Rev. Lett.* **2003**, *90*, 217401.
25. Avouris, P.; Freitag, M.; Perebeinos, V. Carbon-Nanotube Photonics and Optoelectronics. *Nat. Photon.* **2008**, *2*, 341–350.
26. Freitag, M.; Martin, Y.; Misewich, J. A.; Martel, R.; Avouris, P. Photoconductivity of Single Carbon Nanotubes. *Nano Lett.* **2003**, *3*, 1067–1071.
27. Itkis, M. E.; Borondics, F.; Yu, A.; Haddon, R. C. Bolometric Infrared Photoresponse of Suspended Single-Walled Carbon Nanotube Films. *Science* **2006**, *312*, 413–416.
28. Weisman, R. B.; Bachilo, S. M. Dependence of Optical Transition Energies on Structure for Single-Walled Carbon Nanotubes in Aqueous Suspension: An Empirical Kataura Plot. *Nano Lett.* **2003**, *3*, 1235–1238.
29. Rotkin, S. V. Electronic Properties of Nonideal Nanotube Materials: Helical Symmetry Breaking in DNA Hybrids. *Annu. Rev. Phys. Chem.* **2010**, *61*, 241–261.
30. Tu, X.; Manohar, S.; Jagota, A.; Zheng, M. DNA Sequence Motifs for Structure-Specific Recognition and Separation of Carbon Nanotubes. *Nature* **2009**, *460*, 250–253.
31. Torrens, O. N.; Milkie, D. E.; Zheng, M.; Kikkawa, J. M. Photoluminescence from Intertube Carrier Migration in Single-Walled Carbon Nanotube Bundles. *Nano Lett.* **2006**, *6*, 2864–2867.
32. Lefebvre, J.; Finnie, P. Photoluminescence and Förster Resonance Energy Transfer in Elemental Bundles of

Single-Walled Carbon Nanotubes. *J. Phys. Chem. C* **2009**, *113*, 7536–7540.
33. Qian, H.; Georgi, C.; Anderson, N.; Green, A. A.; Hersam, M. C.; Novotny, L.; Hartschuh, A. Exciton Energy Transfer in Pairs of Single-Walled Carbon Nanotubes. *Nano Lett.* **2008**, *8*, 1363–1367.
34. Kato, T.; Hatakeyama, R. Exciton Energy Transfer-Assisted Photoluminescence Brightening from Freestanding Single-Walled Carbon Nanotube Bundles. *J. Am. Chem. Soc.* **2008**, *130*, 8101–8107.
35. Tan, P. H.; Rozhin, A. G.; Hasan, T.; Hu, P.; Scardaci, V.; Milne, W. I.; Ferrari, A. C. Photoluminescence Spectroscopy of Carbon Nanotube Bundles: Evidence for Exciton Energy Transfer. *Phys. Rev. Lett.* **2007**, *99*, 137402.
36. Chen, F.; Ye, J.; Teo, M. Y.; Zhao, Y.; Tan, L. P.; Chen, Y.; Chan-Park, M. B.; Li, L.-J. Species-Dependent Energy Transfer of Surfactant-Dispersed Semiconducting Single-Walled Carbon Nanotubes. *J. Phys. Chem. C* **2009**, *113*, 20061–20065.
37. Qian, H.; Georgi, C.; Anderson, N.; Green, A. A.; Hersam, M. C.; Novotny, L.; Hartschuh, A. Exciton Transfer and Propagation in Carbon Nanotubes Studied by Near-Field Optical Microscopy. *Phys. Status Solidi B* **2008**, *245*, 2243–2246.
38. Koyama, T.; Miyata, Y.; Asada, Y.; Shinohara, H.; Kataura, H.; Nakamura, A. Bright Luminescence and Exciton Energy Transfer in Polymer-Wrapped Single-Walled Carbon Nanotube Bundles. *J. Phys. Chem. Lett.* **2010**, *1*, 3243–3248.
39. Crochet, J. J.; Sau, J. D.; Duque, J. G.; Doorn, S. K.; Cohen, M. L. Electrodynamic and Excitonic Intertube Interactions in Semiconducting Carbon Nanotube Aggregates. *ACS Nano* **2011**, *5*, 2611–2618.
40. Lebedkin, S.; Kareev, I.; Hennrich, F.; Kappes, M. M. Efficient Quenching of Singlet Oxygen via Energy Transfer to Semiconducting Single-Walled Carbon Nanotubes. *J. Phys. Chem. C* **2008**, *112*, 16236–16239.
41. Chen, F.; Zhang, W.; Jia, M.; Wei, L.; Fan, X.-F.; Kuo, J.-L.; Chen, Y.; Chan-Park, M. B.; Xia, A.; Li, L.-J. Energy Transfer from Photo-Excited Fluorene Polymers to Single-Walled Carbon Nanotubes. *J. Phys. Chem. C* **2009**, *113*), 14946–14952.
42. Schuettfort, T.; Snaith, H. J.; Nish, A.; Nicholas, R. J. Synthesis and Spectroscopic Characterization of Solution Processable Highly Ordered Polythiophene−Carbon Nanotube Nanohybrid Structures. *Nanotechnology* **2010**, *21*, 025201.
43. Loi, M. A.; Gao, J.; Cordella, F.; Blondeau, P.; Menna, E.; Bártová, B.; Hébert, C.; Lazar, S.; Botton, G. A.; Milko, M.; *et al*. Encapsulation of Conjugated Oligomers in Single-Walled Carbon Nanotubes: Towards Nanohybrids for Photonic Devices. *Adv. Mater.* **2010**, *22*, 1635–1639.
44. Ahmad, A.; Kern, K.; Balasubramanian, K. Selective Enhancement of Carbon Nanotube Photoluminescence by Resonant Energy Transfer. *ChemPhysChem* **2009**, *10*, 905–909.
45. Magadur, G.; Lauret, J.-S.; Alain-Rizzo, V.; Voisin, C.; Roussignol, P.; Deleporte, E.; Delaire, J. A. Excitation Transfer in Functionalized Carbon Nanotubes. *ChemPhysChem* **2008**, *9*, 1250–1253.
46. Cambré, S.; Wenseleers, W.; Čulin, J.; Van Doorslaer, S.; Fonseca, A.; Nagy, J. B.; Goovaerts, E. Characterisation of Nanohybrids of Porphyrins with Metallic and Semiconducting Carbon Nanotubes by EPR and Optical Spectroscopy. *ChemPhysChem* **2008**, *9*, 1930–1941.
47. Avouris, P.; Chen, J. Nanotube Electronics and Optoelectronics. *Mater. Today* **2006**, *9*, 46–54.
48. Lu, W.; Lieber, C. M. Nanoelectronics from the Bottom Up. *Nat. Mater.* **2007**, *6*, 841–850.
49. Karachevtsev, V. A.; Glamazda, A. Y.; Leontiev, V. S.; Lytvyn, O. S.; Dettlaff-Weglikowska, U. Glucose Sensing Based on NIR Fluorescence of DNA-Wrapped Single-Walled Carbon Nanotubes. *Chem. Phys. Lett.* **2007**, *435*, 104–108.
50. Bunzli, J.-C. G.; Piguet, C. Taking Advantage of Luminescent Lanthanide Ions. *Chem. Soc. Rev.* **2005**, *34*, 1048–1077.
51. Förster, T. Zwischenmolekulare Energie-Wanderung und Fluoreszenz. *Ann. Phys.* **1948**, *2*, 55–75.
52. Dexter, D. L. A Theory of Sensitized Luminescence in Solids. *J. Chem. Phys.* **1953**, *21*, 836–850.
53. Wang, F.; Dukovic, G.; Brus, L. E.; Heinz, T. F. Time-Resolved Fluorescence of Carbon Nanotubes and Its Implication for Radiative Lifetimes. *Phys. Rev. Lett.* **2004**, *92*, 177401.
54. Yamase, T.; Naruke, H. Luminescence and Energy Transfer Phenomena in Tb^{3+}/Eu^{3+}-Mixed Polyoxometallolanthanoates $K_{15}H_3[Tb_{1.4}Eu_{1.6}(H_2O)_3(SbW_9O_{33})(W_5O_{18})_3]\cdot 25.5H_2O$ and $Na_7H_{19}[Tb_{4.3}Eu_{1.7}O_2(OH)_6(H_2O)_6Al_2(Nb_6O_{19})_5]\cdot 47H_2O$. *J. Phys. Chem. B* **1999**, *103*, 8850–8857.
55. Mirochnik, A. G.; Petrochenkova, N. V.; Karasev, V. E. Energy Transfer in Luminescent Complexes of Eu^{III} and Tb^{III} with Homo- and Copolymers of Acrylic Acid and Alkyl Methacrylates. *Russ. Chem. Bull.* **1996**, *45*, 1356–1359.
56. Xiao, Y. F.; Nhan, T. Q.; Wilson, M. W. B.; Fraser, J. M. Saturation of the Photoluminescence at Few-Exciton Levels in a Single-Walled Carbon Nanotube under Ultrafast Excitation. *Phys. Rev. Lett.* **2010**, *104*, 017401.
57. Berciaud, S.; Cognet, L.; Lounis, B. Luminescence Decay and the Absorption Cross Section of Individual Single-Walled Carbon Nanotubes. *Phys. Rev. Lett.* **2008**, *101*, 077402.
58. Islam, M. F.; Milkie, D. E.; Kane, C. L.; Yodh, A. G.; Kikkawa, J. M. Direct Measurement of the Polarized Optical Absorption Cross Section of Single-Wall Carbon Nanotubes. *Phys. Rev. Lett.* **2004**, *93*, 037404.
59. Tsyboulski, D. A.; Rocha, J.-D. R.; Bachilo, S. M.; Cognet, L.; Weisman, R. B. Structure-Dependent Fluorescence Efficiencies of Individual Single-Walled Carbon Nanotubes. *Nano Lett.* **2007**, *7*, 3080–3085.
60. Carlson, L. J.; Maccagnano, S. E.; Zheng, M.; Silcox, J.; Krauss, T. D. Fluorescence Efficiency of Individual Carbon Nanotubes. *Nano Lett.* **2007**, *7*, 3698–3703.
61. Elbanowski, M.; Lis, S.; Konarski, J. Quantum Efficiency of the Luminescence of Eu(III), Tb(III), and Dy(III) in Aqueous Solutions. *Monatsh. Chem./Chem. Monthly* **1989**, *120*, 699–703.
62. Zheng, M.; Jagota, A.; Semke, E. D.; Diner, B. A.; McLean, R. S.; Lustig, S. R.; Richardson, R. E.; Tassi, N. G. DNA-Assisted Dispersion and Separation of Carbon Nanotubes. *Nat. Mater.* **2003**, *2*, 338–342.
63. Bachilo, S. M.; Balzano, L.; Herrera, J. E.; Pompeo, F.; Resasco, D. E.; Weisman, R. B. Narrow (n,m)-Distribution of Single-Walled Carbon Nanotubes Grown Using a Solid Supported Catalyst. *J. Am. Chem. Soc.* **2003**, *125*, 11186–11187.
64. Lolli, G.; Zhang, L.; Balzano, L.; Sakulchaicharoen, N.; Tan, Y.; Resasco, D. E. Tailoring (n,m) Structure of Single-Walled Carbon Nanotubes by Modifying Reaction Conditions and the Nature of the Support of CoMo Catalysts. *J. Phys. Chem. B* **2006**, *110*, 2108–2115.